# Asynchronous Multiple-Access for Low-Latency Communications and Related Waveforms

Woojin Park

Department of Electrical Engineering

Graduate School of UNIST

# Asynchronous Multiple-Access for Low-Latency Communications and Related Waveforms

A thesis/dissertation
submitted to the Graduate School of UNIST
in partial fulfillment of the
requirements for the degree of
Master of Science

Woojin Park

12. 16. 2016

Approved by

Advisor
Hyun Jong Yang

# Asynchronous Multiple-Access for Low-Latency Communications and Related Waveforms

Woojin Park

This certifies that the thesis/dissertation of Woojin Park is approved.

12. 16. 2016

signature

Advisor: Hyun Jong Yang

signature

Jin-Ho Chung: Thesis Committee Member #1

signature

Hyoil Kim: Thesis Committee Member #2

**Abstract**

For fulfilling the requirements of real-time communications, wireless communication system has to have ultra-low latency performance, namely latency less than 1ms. However, current cellular network with synchronous multiple-access, such as Long-Term Evolution(LTE), has fundamental limits to accomplish the requirement.

In this thesis, asynchronous multiple-access, and related waveform, generalized frequency division multiplexing(GFDM), are studied as one of the alternatives. In the numerical analysis, GFDM and conventional modulation methods, such as single carrier frequency-division multiple-access(SC-FDMA) and orthogonal frequency-division multiplexing(OFDM) modulations, are compared in the asynchronous uplink multiple-access environment with both link-level simulation(LLS) and system-level simulation(SLS). In the comparison, GFDM shows greater performance in the high signal-to-noise ratio(SNR) regime due to the better out-of-band emission performance than conventional modulation methods.

# Contents

# List of Figures

# List of Tables

## Nomenclature

| | |
|---|---|
| 5G | fifth generation |
| AWGN | additive white Gaussian noise |
| BER | bit error rate |
| BS | base station |
| ERC | extended raised cosine |
| GFDM | generalized frequency division multiplexing |
| i.i.d. | independent and identically distributed |
| IFT | inverse Fourier transform |
| ITU-R | The International Telocommunication Union - recommendation section |
| LLS | link-level simulation |
| LTE | Long-Term Evolution |
| OFDM | orthogonal frequency-division multiplexing |
| OFDMA | orthogonal freuqency-division multiple-access |
| OOBE | out-of-band emission |
| PSD | power spectral density |
| QAM | quadrature amplitude modulation symbol |
| RB | resource block |
| RC | raised cosine |
| SC-FDMA | single carrier frequency-division multiple-access |
| SINR | signal-to-interference-plus-noise ratio |
| SLS | system-level simulation |
| TTI | transmission-time-interval |
| UE | user equipment |
| ZF | zero-forcing |

# 1 Introduction

One of the prominent contents in the fifth generation(5G) wireless communication is real-time applications, such as streaming gaming, tactile internet, remote surgery, and augmented reality [14, 13, 10]. For these applications to become feasible, the wireless communication system has to satisfy highly-demanding requirements on ultra-low latency. The International Telecommunication Union recommendation section(ITU-R) suggests that the latency on the physical layer of the 5G network should be less than 1ms [6, 1].

However, current cellular network, Long-Term Evolution(LTE), has excessive delay, hence cannot follow the recommendation. For example, in the LTE system, the minimum transmittable unit of signal is set to be 1ms, which implies the processing on the unit may yield further delay. For another example, the uplink transmission in LTE requires at least 8ms from the scheduling request to data transmission [9, 5, 8].

To overcome fundamental delay limit in synchronous multiple-access, an asynchronous approach for the 5G mobile communications uplink has been discussed [14, 18]. However, asynchronous multiple-access has its deficit in that the adjacent sub-bands can be interfered by the out-of-band emission (OOBE) Thus, the key criterion of the waveforms for asynchronous multiple-access is low OOBE appearance [23, 21, 19].

One of the prospective modulation methods is generalized frequency division multiplexing(GFDM). The concept of GFDM was first introduced in [12]. The bit error rate(BER) performance is presented in [24, 19], in particular, OOBE performance is discussed in [19]. In [15], the low-complexity transceiver structure is introduced and the comprehensive explanation about GFDM is collected in [25].

In this thesis, asynchronous multiple-access and GFDM modulation is introduced, then numerical analysis on comparison between GFDM and conventional modulation methods are compared in asynchronous multiple-access with three different simulation models. In the Sections 3 and 4, the GFDM modulation performance is numerically measured in asynchronous multiple-access environment with two link-level simulation(LLS): simulation with additive white Gaussian noise(AWGN) channel and frequency selective channel. The achievable sum-rate or spectral efficiency of GFDM modulation and single carrier frequency-division multiple-access(SC-FDMA) modulation are compared.In the section 5, GFDM and orthogonal frequency-division multiplexing(OFDM) are numerically analyzed by system-level simulation(SLS) where the asynchronous uplink multiple-access and the small cell scenario are assumed.

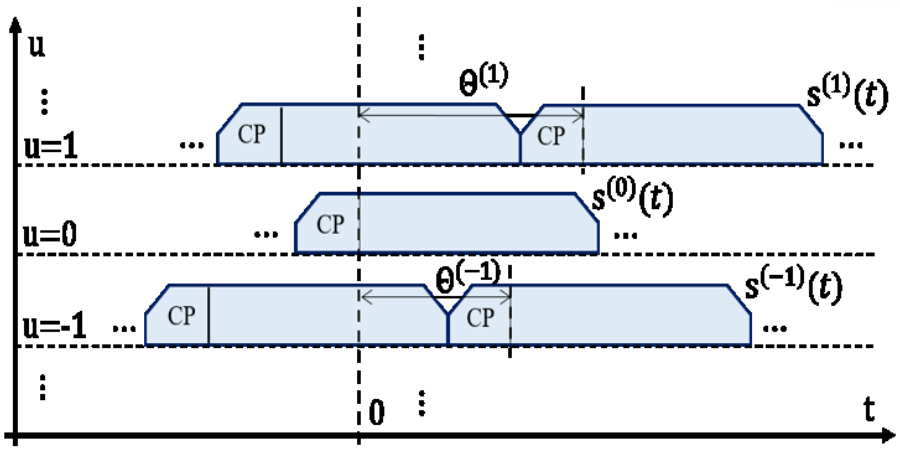


Figure 1: Signal transmission in asynchronous multiple-access.

# 2 Asynchronous uplink multiple-access and waveforms

## 2.1 Asynchronous multiple-access

In the asynchronous multiple-access scheme in this thesis, a user equipment(UE) transmits signal to the base station(BS) via a sub-band without synchronization among the signals via the other sub-bands. Transmission of signals in asynchronous multiple-access is illustrated in figure 1. In figure 1, $u$ represents index of a user, hence signal from user $u$ is denoted by $s^{(u)}(t)$. The signals from different UE is asynchronously transmitted with time offset, $\Theta^{(u)}$ , which is explained in 2.2.

When there exist data to transmit in the UE, the prompt transmission reduces latency compared to synchronous multiple-access by following reasons. First, signals in the asynchronous multiple-access scheme does not have to wait the time slot for synchronization of the data for transmission. The waiting delay can be also reduced in synchronous multiple-access, but it requires the shortening of the transmit-time-interval(TTI).

Second, user scheduling process is skipped on the asynchronous multiple-access scheme. Current LTE system requires more than 8ms of duration on the scheduling process. Although the scheduling delay might be reduced by shortened TTI, there still exist processing delay for resource allocation at BS side. On the other hand, the transmission without user scheduling in synchronous multiple-access is hard to be implemented since timing advance on the scheduling process can not exploited. The asynchronous multiple-access scheme reduces this user scheduling delay.

In the asynchronous multiple-access scheme, the orthogonality of subcarriers of multiple UE's signals is not preserved whereas synchronous multiple-access such as orthogonal frequency-division multiple-access(OFDMA) exploits the orthogonality for high throughput. Therefore the low OOBE is important to reduce the interference due to the non-orthogonality among sub-bands.

GFDM signal is a waveform having lower OOBE than conventional multi-carrier modulated signals such as OFDM and SC-FDMA signals. In the following subsections, conventional waveforms

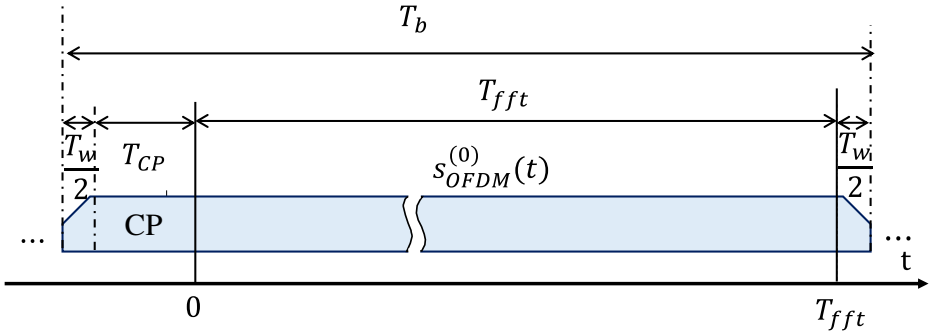


Figure 2: One OFDM symbol block in time-domain.

and GFDM waveform are introduced and compared.

## 2.2 The OFDM and SC-FDMA waveforms

The continuous-time signal of OFDM is generated by mapping of symbols on subcarriers. On the base-band representation, a subcarrier shaped as the Dirac delta function $\delta(f - f')$ in frequency-domain is equivalent to the infinite length of time-domain signal shaped as $e^{j2\pi f' t}$ where $j = \sqrt{-1}$, $f$ is the frequency-domain variable, $f'$ is the frequency shift of the subcarrier, and $t$ is the time-domain variable. Since the OFDM signals have to deliver different symbols in different time invervals, the complex periodic signal is truncated by limited-time window function $w(t)$ [30, 11, 17]. The detailed description about the window function, $w(t)$ , shall be explained in the Section 2.3

Let $T_{fft}$, $T_{CP}$, and $T_w$ denote the time duration of one period of the sinusoidal signal drawn by fundamental frequency of subcarrier frequencies, the time duration of CP, and the time extension by the extended-raised-cosine(ERC) window respectively as illustrated in figure 2. The sum, the time duration for a symbol block $T_b$, is calculated as $T_b = T_{fft} + T_{CP} + T_w$ on OFDM signal.

Assume that there exist multiple non-overlapping OFDM symbol blocks in time-domain, then a symbol block indicated by time-domain index $l$, $\in \mathbb{Z}$ where $\mathbb{Z}$ represents the set of all integers, and $a * b$ represents continuous convolution operation between $a$ and $b$. The base-band continuous-time representation of the $l$-th OFDM signal in time-domain for user $u$, $s^{(u)}_{l,OFDM}(t)$, is given as [30]

$$s^{(u)}_{l,OFDM}(t) = \left( \sum_{k \in \mathbb{K}^{(u)}} \sqrt{P_{Tx}} d^{(u)}_{l,k} \cdot e^{j2\pi \frac{k}{T_{fft}} t} \cdot w(t) \right) * \delta(t - lT_b - \Theta^{(u)}) \quad (1)$$

$$= \sum_{k \in \mathbb{K}^{(u)}} \sqrt{P_{Tx}} d^{(u)}_{l,k} \cdot e^{j2\pi \frac{k}{T_{fft}} (t - lT_b - \Theta^{(u)})} \cdot w(t - lT_b - \Theta^{(u)}), \quad (2)$$

where $\mathbb{K}^{(u)}$ represents the set of indices of subcarriers which are allocated to user $u$, $k$ is the subcarrier index, $d_{l,k}$ represents unit power quadrature amplitude modulation(QAM) symbol on subcarrier $k$ in the symbol block $l$, $P_{Tx}$ represents per-symbol transmit power, and $\Theta^{(u)}$ , $\in [0, T_b)$,

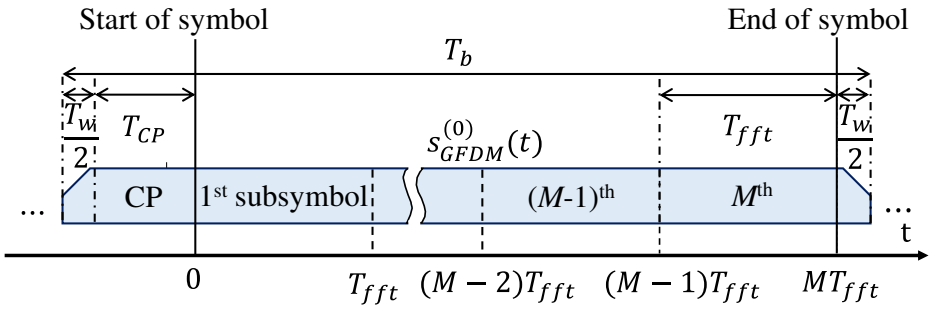


Figure 3: One GFDM symbol block in time-domain.

represents the offset of the starting point of the data, or non-CP, part of the $u$-th symbol block as described in figure 1. That is, if $l = 0$, the starting point of the non-CP part is calibrated at $\Theta^{(u)}$ for user $u$; the figure 2 shows the 0-th OFDM symbol block where $\Theta^{(0)} = 0$. Here, $\mathbb{K}^{(u)}$ is composed with consecutive $K$ indices indicating consecutive subcarriers in frequency-domain, which means the subcarriers are clustered within a band. Note that the carrier spacing is determined as $1/T_{fft}$.

The $l$-th SC-FDMA signal[1] symbol for $u$-th user, $s^{(u)}_{l,SC-FDMA}(t)$, is generated in the similar method to the OFDM signal, but symbols for mapping on the subcarriers are the output of DFT of the original input symbols. Let $\mathbf{d}^{(u)}_l = [d^{(u)}_{l,k^{(u)}_{min}} \; d^{(u)}_{l,k^{(u)}_{min}+1} \cdots d^{(u)}_{l,k^{(u)}_{max}}]^T$, where $k^{(u)}_{min}$ and $k^{(u)}_{max}$ represent the minimum and the maximum subcarrier indices in $\mathbb{K}^{(u)}$ respectively, and the operation $[\cdot]^T$ represents transpose of the vector $[\cdot]$. The signal, $s^{(u)}_{l,SC-FDMA}(t)$, is then given as [26, 27].

$$s^{(u)}_{l,SC-FDMA}(t) = \sum_{k \in \mathbb{K}^{(u)}} \sqrt{P_{Tx}} [\mathbf{D}_K \mathbf{d}^{(u)}_l]_{k-k^{(u)}_{min}+1,1} \cdot e^{j2\pi \frac{k}{T_{fft}}(t - lT_b - \Theta^{(u)})} \cdot w(t - lT_b - \Theta^{(u)}), \quad (3)$$

where $\mathbf{D}_K$, $\in \mathbb{C}^{K \times K}$, is DFT matrix for $K$ parameters, and $[\cdot]_{a,b}$ represents $(a, b)$-th component of matrix $\cdot$.

### 2.3 The GFDM waveform

One GFDM symbol block consists of $M$ GFDM subsymbols in the time-domain as shown in figure 3. Each GFDM subsymbol contains $K$ subcarriers in the frequency-domain, and is distinguished by multiplication of circularly shifting time-domain *GFDM waveform function*.

[1] In asynchronous multiple-access, the name, *SC-FDMA signal*, is contradict since the SC-FDMA is a multiple-access scheme with synchronized transmission for every users. However, the modulating method and corresponding signals employing DFT spreading before OFDM still has to be differentiated from the OFDM although the multiple-access scheme is not SC-FDMA. Therefore, when the term *SC-FDMA signal* is used, the actual meaning, hereafter, is not the multiplexing of the multiple signals on the SC-FDMA scheme, but the signal that employs QAM mapping by OFDM after DFT spreading. The term *SC-FDMA signal* is also used in the 3GPP specifications by this sense, particularly in [5, 7].

The GFDM waveform function in time-domain is defined as [19, 25, 28]

$$v(t) = \mathcal{F}^{-1}\left\{ \sum_{q=-\infty}^{\infty} V_{filt}\left(\frac{q}{MT_{fft}}\right) \delta\left(f - \frac{q}{MT_{fft}}\right) \right\}, \tag{4}$$

where $\mathcal{F}^{-1}(O(f))$ means the inverse Fourier transform (IFT) of a function $O(f)$ in the frequency-domain, $V_{filt}(f)$ is the spectrum filter such as raised cosine(RC), root raised cosine, 1st Xia, and 4th Xia functions [31, 25]. It is notable that maximum $2M$ frequency points are non-zero depending on the roll-off factor of the filters in (4) [25]. If the function $v(t)$ moves along time-domain, the frequency-domain representation, which is the terms inside the IFT function, shows phase shifting from the original frequency representation of $v(t)$. On the simulation in this thesis, the RC filter is determined with roll-off factor $\alpha = 0.5$, i.e.,

$$V_{filt}(f) = \frac{1}{2}\left(1 - \cos\left(\pi \mathrm{lin}_{\alpha}\left(\frac{f}{M}\right)\right)\right), \tag{5}$$

where, $\mathrm{lin}_{\alpha}(x) = \min[1, \max\{0, (1-\alpha)/2\alpha - |x|/\alpha\}]$ [25, 31, 28].

As a result, shape of one GFDM signal is shaped as the concatenation of $M$-OFDM data parts multiplied by $M$ distinguishable GFDM waveform functions with the length of GFDM data part is equivalent to $MT_{fft}$. The total time duration $T_b$, thus, is calculated as $T_b = MT_{fft} + T_{CP} + T_w$ for one GFDM symbol block as depicted in figure 3.

In consequence, the GFDM pulse shape to convey the $l$-th QAM symbol on $k$-th subcarrier and $m$-th subsymbol of user $u$, $g^{(u)}_{l,k,m}(t)$, is defined as

$$g^{(u)}_{l,k,m}(t) = e^{j2\pi\frac{k}{T_{fft}}t} v\left(t - mT_{fft} - lT_b - \Theta^{(u)}\right) \cdot w\left(t - lT_b - \Theta^{(u)}\right) \tag{6}$$

where $k \in \mathbb{K}^{(u)}$, and $m \in \{0, 1, \cdots, M\}$. Let $d^{(u)}_{l,k,m}$ denotes the unit-power QAM symbol of the $l$-th symbol block, $k$-th subcarrier, and $m$-th GFDM subsymbol of user $u$. The GFDM signal for $l$-th symbol block for user $u$, then, is generated as

$$s^{(u)}_{l,GFDM}(t) = \sum_{m=0}^{M-1} \sum_{k \in \mathbb{K}^{(u)}} g^{(u)}_{l,k,m}(t) \cdot d^{(u)}_{l,k,m}. \tag{7}$$

The vector of QAM symbols in $l$-th symbol block of user $u$ for GFDM is defined as

$$\mathbf{d}^{(u)}_l = [\ d^{(u)}_{l,k_{min},0} \quad \cdots \quad d^{(u)}_{l,k_{min},0} \quad d^{(u)}_{l,k_{min},1} \quad \cdots \quad d^{(u)}_{l,k_{max},M-1}\ ]^T. \tag{8}$$

The notation of the vectors of QAM symbols for OFDM/SC-FDMA and GFDM can be unified to be $\mathbf{d}^{(u)}_l$ in 8 given that the number of GFDM subsymbol, $M$, is set to be 1 for OFDM/SC-FDMA signals. Hereafter, unified denotation of $\mathbf{d}^{(u)}_l$ is used for convenience.

One of two window functions is multiplied on (1), (3), and (6): Either CP-window or ERC-

Table 1: Window functions

| Window | Time-domain | Frequency-domain |
|---|---|---|
| CP-window | $w(t) = \text{Rect}\left(\frac{t-\Delta T}{T_{data}}\right)$ | $W(f) = T_{data} \cdot \text{sinc}(T_{data} f) \cdot e^{-j2\pi\Delta T f}$ |
| ERC-window | $w(t) = \text{Rect}\left(\frac{t-\Delta T}{T_b}\right) * \left\{\frac{\pi}{2T_w} \cdot \text{Rect}\left(\frac{t}{T_w}\right) \cdot \cos\left(\frac{\pi}{T_w} t\right)\right\}$ | $W(f) = T_b \cdot \text{sinc}(T_b f) * \left\{\frac{\cos(\pi T_w f)}{1-4T_w^2 f^2}\right\} \cdot e^{-j2\pi\Delta T f}$ |

window. A CP-added signal, on one hand, can be designed by insertion of some last part of the signal in front of the signal. On the other hand, the CP-added signal can be obtained by truncation of the infinitely spanning periodic signal assumed in the front of the Section 2.2. In the latter case, the truncation is operated by multiplication of rectangular-shaped function. This rectangular function, $\text{Rect}(\cdot)$ is defined as

$$\text{Rect}(x) = \begin{cases} 1, & x \in (-0.5, 0.5) \\ 0.5, & x = -0.5 \text{ or } 0.5 \\ 0, & \text{otherwise.} \end{cases} \tag{9}$$

of which the length of support, $T_{data}$, is equivalent to $T_{fft}+T_{CP}$ for OFDM/SC-FDMA and $MT_{fft}+T_{CP}$ for GFDM.

The ERC-window has been invented to reduce the OOBE. Instead of using CP-window, the use of ERC-window enables to show lower OOBE, particularly where many guard subcarriers are inserted between the transmitting sub-band and receiving sub-band as shown in figure 4. The window functions are defined in table 1. In the table 1, the point of the center of the block $\Delta T = (T_{data} - 2T_{CP})/2$. The OOBE is covered by the next subsection.

### 2.4 Out-of-band emission analysis

Assuming a signal is being transmitted via band $i$, the bandwidth outside, but adjacent to, the band $i$ has the spectrum emitted by the transmission via the band $i$. In the case of multiple-access with synchronization, such as OFDMA and SC-FDMA, the OOBE is nullified at the subcarriers on which QAM symbols are transmitted. However in asynchronous multiple-access, the OOBE of transmission in one band does affects on subcarriers in the other bands, thus the neighboring channels are degenerated by the interference as described in figure 5 [19, 18, 20, 22].

OOBE of a signal can be given with derivation of power spectral density(PSD) of the signal. PSD of random process $X(t)$ is, in words, *the mean throughout the infinite time span of expectation of square of frequency representation of the random process $X(t)$,* or, more intuitively, *the expectation of time average of spectral power.* As an equation, PSD of time-domain signal, $X(t)$, is derived as

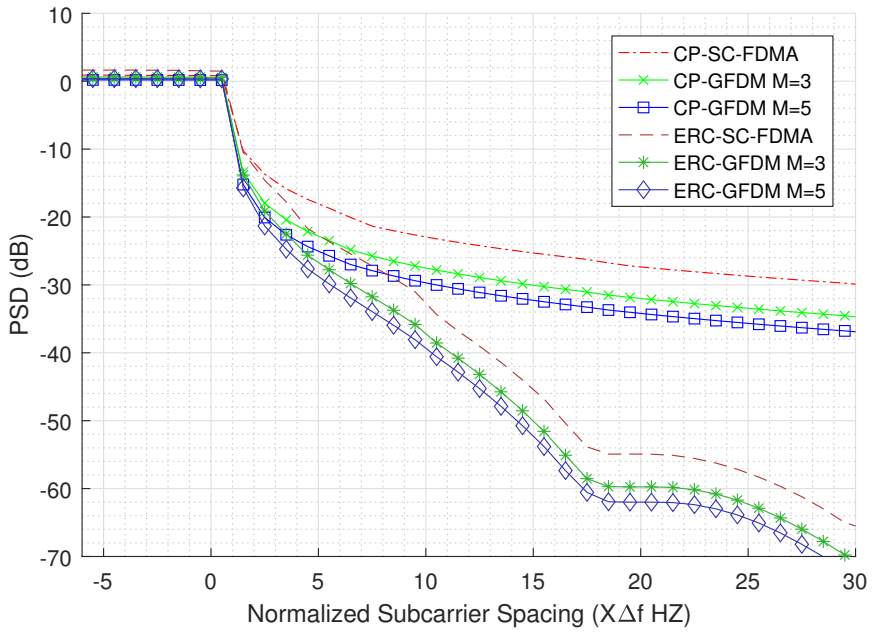


Figure 4: Out-of-band emission of OFDM/SC-FDMA and GFDM..

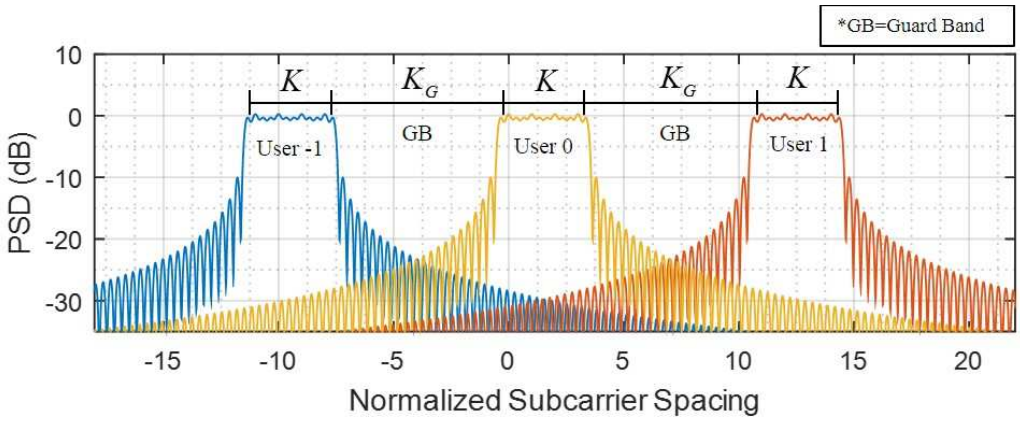


Figure 5: Inter-user interference by out-of-band emission in asynchronous multiple-access. Power spectral density of GFDM with 4 subcarriers, 3 GFDM subsymbols, and 7 guard subcarriers.

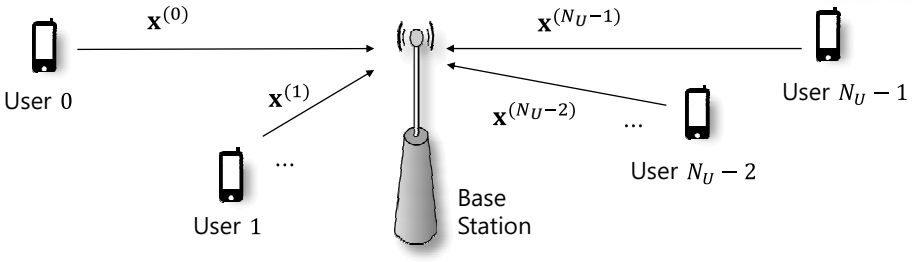


Figure 6: Nodes in asynchronous multiple-access.

[16, 29]

$$\mathrm{PSD}_X(f) = \lim_{T\to\infty} \frac{1}{T}\mathrm{E}\left[\left|\mathrm{Rect}(\frac{t}{T})X(t)\right|^2\right]. \tag{10}$$

The PSD of OFDM is given as

$$\mathrm{PSD}_{OFDM}(f) = \frac{P_{Tx}}{T_b}\sum_k \left|W\left(f-\frac{k}{T_{fft}}\right)^2\right|, \tag{11}$$

for the arbitrary set of subcarriers indicated by $k$. The power spectral density of the SC-FDMA signal is the same with that of OFDM.

The PSD of GFDM is obtained as

$$\mathrm{PSD}_{GFDM}(f) = \frac{P_{Tx}}{(MT_{fft})^2 T_b}\sum_k \sum_{m=0}^{M-1}\left|\sum_{p=-M}^{M} G_{filt}\left(\frac{p}{MT_{fft}}\right) W\left(f-\frac{p}{MT_{fft}}-\frac{k}{T_{fft}}\right) e^{-j2\pi\frac{m}{M}p}\right|^2, \tag{12}$$

The comparison between OOBE of OFDM/SC-FDMA and GFDM signals are drawn in figure 4. It is observed the OOBE performance is enhanced as the number of subsymbol increases, and when the ERC-window is used.

# 3 Simulation with AWGN channel.

In this section, sum-rate of the asynchronous uplink multiple-access scheme is numerically analyzed with two different waveforms: GFDM signal and SC-FDMA signal.

## 3.1 System Model

It is assumed that $N_U$ users are equally allocated with a sub-band consisting of $K$ consecutive subcarriers out of the total subcarriers, $K_T$. Between two neighboring sub-bands, a guard band is inserted as depicted in figure 5. Hence, the total number of guard bands is $N_U - 1$.

The block diagram of SC-FDMA and GFDM signal transceiver model is drawn in figure 7. Since the signal of *multiple symbol blocks* in time-domain is generated by independent and identically

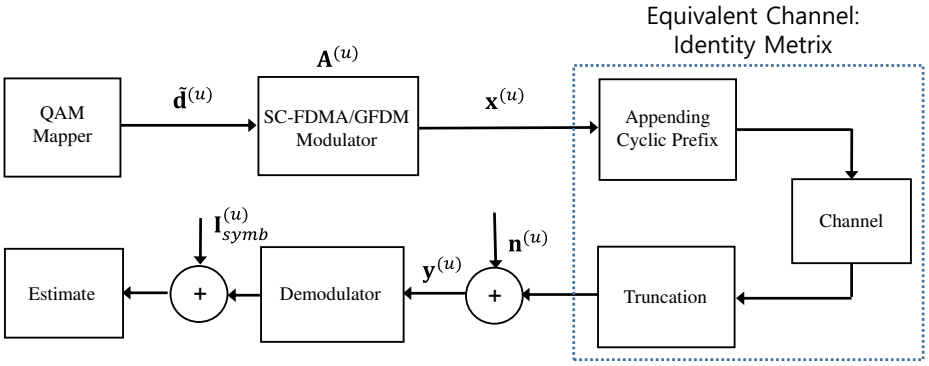


Figure 7: Block diagram of SC-FDMA/GFDM modulation transceiver in asynchronous multiple-access in AWGN channel.

distributed(i.i.d.) QAM symbols, the calculation of throughput on these blocks can be replaced by the calculation of throughput on *multiple trial of the* generation of the 0-th symbol block. Therefore, the symbol block index alone time-domain, $l$, in this section, is dropped. The the vector of QAM symbols for user $u$ can be represented as

$$\mathbf{d}^{(u)} = [\ d^{(u)}_{k^{(u)}_{min},0} \quad \cdots \quad d^{(u)}_{k^{(u)}_{max},0} \quad d^{(u)}_{k^{(u)}_{min},1} \quad \cdots \quad d^{(u)}_{k^{(u)}_{max},M-1}\ ]^T, \tag{13}$$

similar to (8). The vector of the QAM symbols for SC-FDMA signals is given by DFT-spread on $\mathbf{d}^{(u)}$, i.e., $[\mathbf{d}^{(u)}_{SC}]_{k,1} = [\mathbf{D}_K \mathbf{d}^{(u)}]_{k,1}$ where $k \in \mathbb{K}^{(u)}$ [26, 27].

A user only conveys symbols corresponding to $k \in \mathbb{K}^{(u)}$, but the rest symbols in the whole bandwidth out of the selected subcarriers are allocated to the other users. In other words, zero symbols have to be transmitted in the non-selected bands on the modulation, i.e.,

$$[\tilde{\mathbf{d}}^{(u)}]_{i+k_{min},1} = \begin{cases} [\mathbf{d}^{(u)}]_{i,1}, & \text{if } i + k^{(u)}_{min} \in \mathbb{K}^{(u)} \text{ for } i = 0,\, 1,\, \cdots,\, K-1 \\ 0, & \text{otherwise.} \end{cases} \tag{14}$$

For SC-FDMA signal the vector of the zero-padded QAM symbols can be given by substitution of $\mathbf{d}^{(u)}$ by $\mathbf{d}^{(u)}_{SC}$ in (14).

The discrete-time transmit signal from user $u$ to the BS, $\mathbf{x}^{(u)} \in \mathbb{C}^{K_T M \times 1}$, is generated by multiplication between the modulation matrix throughout the whole bandwidth, $\tilde{\mathbf{A}} \in \mathbb{C}^{K_T M \times K_T M}$, and $\tilde{\mathbf{d}}^{(u)}$, i.e.,

$$\mathbf{x}^{(u)} = \tilde{\mathbf{A}} \tilde{\mathbf{d}}^{(u)}. \tag{15}$$

Although $\mathbf{x}^{(u)}$ contains symbols in $K$ subcarriers among $K_T$ subcarriers in the whole bandwidth, $K_T M$ sampling points are required on rows of $\mathbf{A}$ to avoid aliasing. In the case of SC-FDMA modulations, $M = 1$, and the $\tilde{\mathbf{A}}$ is replaced by inverse DFT matrix given as $\mathbf{D}^H_{K_T}$.

The GFDM modulation matrix is given by sampling of the GFDM pulse shape in (6) [25, 15, 29]. The $i$-th column of $\tilde{\mathbf{A}}$ is scalar-multiplied by the $i$-th symbol in $\tilde{\mathbf{d}}^{(u)}$ yielding discrete time signal

for the $i$-th symbol. Hence $\tilde{\mathbf{A}}$ is defined as

$$[\tilde{\mathbf{A}}]_{n,i} = g^{(u)}_{l,k,m}(nT_s), \tag{16}$$

where $i = mK_T + k + 1$, $k \in \mathbb{K}^{(u)} = \{0, 1, \cdots, K_T - 1\}$, $m \in \{0, 1, \cdots, M-1\}$, and $n$ indicates the discrete time point with sampling period $T_s$. The sampling period is given by $\frac{T_{fft}}{K}$ both in SC-FDMA and GFDM signals.

With the AWGN channel assumption, the received signal $\mathbf{y}^{(u)}$ from user $u$, before the consideration of the inter-user interference, is obtained as

$$\mathbf{y}^{(u)} = \mathbf{x}^{(u)} + \mathbf{n}^{(u)}, \tag{17}$$

where $\mathbf{n}^{(u)}$ is the vector of AWGN on user $u$ with variance $\sigma_0^2$.

In this section, the received signal does not contain the inter-user interference by OOBE of other users. The $KM$-dimensional vector of inter-user interference on user $u$, $\mathbf{I}^{(u)}_{symb}$ in figure 7, is considered after demodulation of the received signal from user $u$ with an assumption that the interference term is following the normal distribution.

### 3.2 Interference calculation

The $(k+1)$-th element of $\mathbf{I}^{(u)}_{symb}$ represents the sum of interference on the $k$-th subcarrier of user $u$ received due to the OOBE from the transmission in adjacent sub-bands, where $k \in \{0, 1, \cdots, K-1\}$. It is assumed that $\mathbf{I}^{(u)}_{symb}$ is independent normal random variable with variance $\sigma^{2(u,k)}_{\mathbf{I}}$. The variable $\rho^{(u,k)}$ is calculated by adding out-of-band PSD values at the subcarrier $k$ from the adjacent sub-bands. Since the dominant sources of the inter-user interference are neighboring two bands as illustrated in figure 5, the value of $\sigma^{2(u,k)}_{\mathbf{I}}$ can be approximated as

$$\sigma^{2(u,k)}_{\mathbf{I}} = \begin{cases} \mathrm{PSD}\left(\frac{K+K_G^{(u-1)}+k}{T_{fft}}\right) + \mathrm{PSD}\left(\frac{2K+K_G^{(u)}-(k+1)}{T_{fft}}\right), & u \in \{2, 3, \cdots, N_U - 1\} \\ \mathrm{PSD}\left(\frac{K+K_G^{(u-1)}+k}{T_{fft}}\right), & u = N_U \\ \mathrm{PSD}\left(\frac{2K+K_G^{(u)}-(k+1)}{T_{fft}}\right) & u = 1 \end{cases} \tag{18}$$

where, $K_G^{(u)}$ is the number of guard subcarriers between $u$-th and $(u+1)$-th sub-bands. The PSD function in (18) represents either PSD function of OFDM/SC-FDMA signal in (11) or that of GFDM signal in (12).

Table 2: Parameters of simulation on AWGN

| Item | Value |
|---|---|
| One OFDM data duration ($T_{fft}$) | 66.7$\mu$s |
| Cyclic prefix length ($T_{CP}$) | 4.7$\mu$s |
| Additional time for ERC-window ($T_w$) | 4.7$\mu$s |
| Number of subcarriers in the system ($K_T$) | 100 |
| Subcarrier spacing | 15kHz |
| Bandwidth | 15MHz |

### 3.3 Throughput calculation

From the sum-rate result for the SC-FDMA with minimum mean-square error(MMSE) receiver [27], the sum-rate of SC-FDMA signal with inter-user interference is given as

$$R_{SC-FDMA} = \frac{N_U}{T_b}\log\left\{1+\left(\frac{1}{\frac{1}{K}\sum_{k\in\mathbb{K}^{(u)}}\frac{P_{tr}}{P_{tr}+\sigma_0^2+\sigma_{\mathbf{I}}^{2(u,k)}}}-1\right)\right\} \tag{19}$$

With the zero-forcing receiver, the sum-rate of the GFDM is expressed as

$$R_{GFDM} = \frac{N_U}{T_b}\sum_{m=0}^{M-1}\sum_{k\in\mathbb{K}^{(u)}}\log\left(1+\frac{P_{tr}}{\sigma_0^2\left[\mathbf{A}^{-1}\mathbf{A}^{-\mathrm{H}}\right]_{i,i}+\sigma_{\mathbf{I}}^{2(u,k)}}\right), \tag{20}$$

where $i = mK + k + 1$, $k \in \{0, 1, \cdots, K\}$, and $m \in \{0, 1, \cdots, M\}$.

### 3.4 Numerical results

The system parameters considered in the simulations are summarized in table 2. In addition, the number of subcarriers per guard band, $K_G^{(u)}$, is assumed to be constant as

$$K_G^{(u)} = \left\lfloor \frac{K_T - KN_U}{N_U - 1} \right\rfloor, \tag{21}$$

where $\lfloor a \rfloor$ means the largest integer which is smaller or equal to $a$.

Figure 8a shows the sum-rates versus signal-to-noise ratio for $K = 12$, $K_G = 2$, and $N_U = 6$. It is observed that in the high SNR regime, where the inter-user interference due to non-zero OOB emission is dominant to noise, the family of GFDM modulation exhibit higher sum-rates than SC-FDMA modulation. The ERC-windowing in table 1 provides significant sum-rate gain for both SC-FDMA and GFDM signals. As $M$ increases in GFDM, the sum-rate increases due to the reduced portion of CP duration and reduced OOBE.

Figure 8b shows the same results as in figure 4 (a), but is enlarged for the practical SNR range of 0 to 18 dB. It is seen that for the low to mid SNR regime, i.e., 0 to 12 dB, where the noise

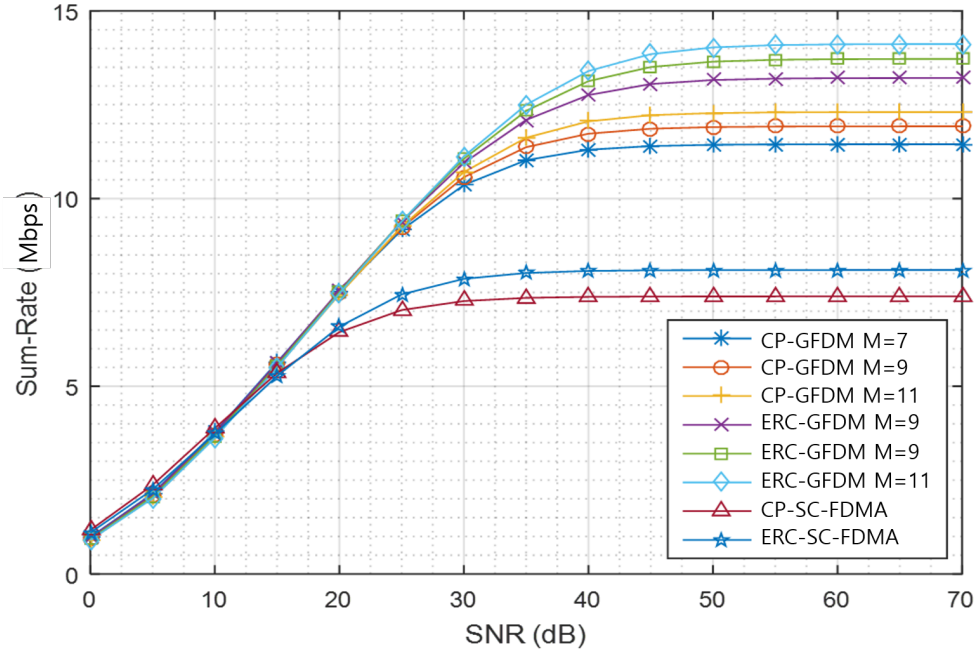


(a)

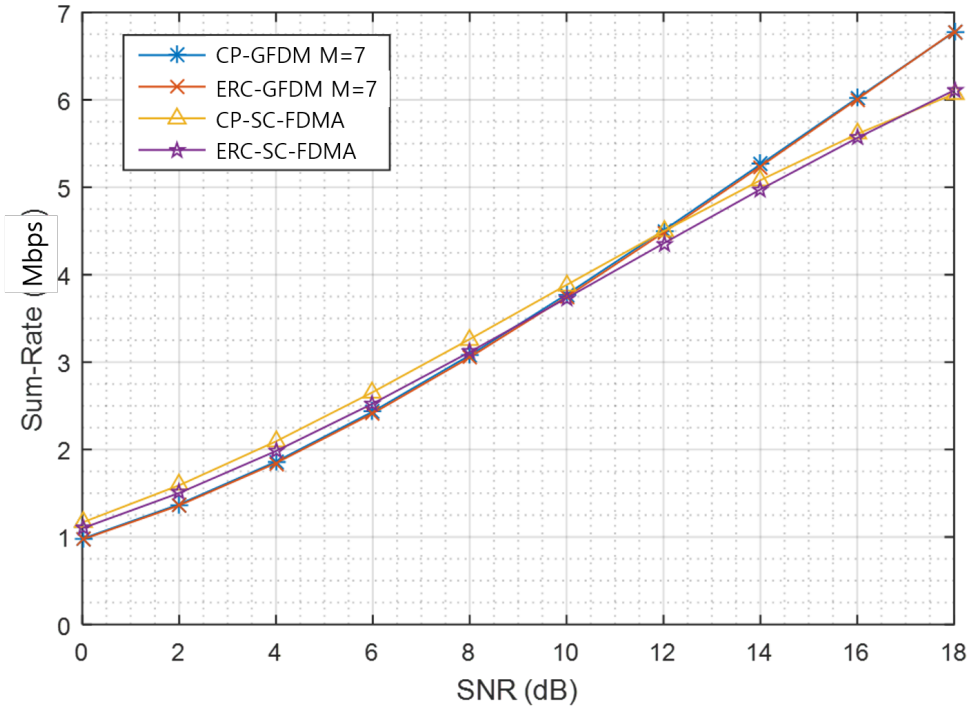


(b)

Figure 8: Sum-rates vs. signal-to-noise ratio(SNR) with 12 subcarriers, 2 guard subcarriers, and 6 users for SNR intervals: (a) 0dB to 70dB and (b) 0dB to 18dB.

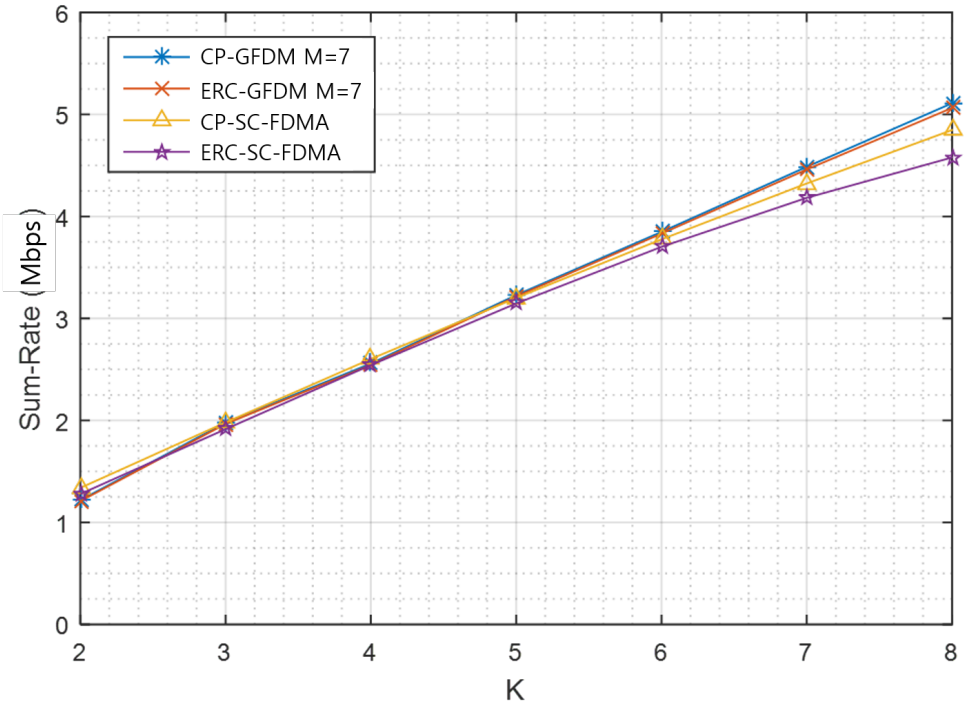


Figure 9: Sum-rates vs. number of subcarriers with 12dB of signal-to-noise ratio and 12 users.

is dominant, SC-FDMA signals show the better sum-rates. However, beyond 12dB of SNR, the GFDM modulation shows better sum-rates than the SC-FDMA modulation due to reduced OOBE.

Figure 9 shows the sum-rates vs. $K$ where SNR=12dB and $N_U = 12$. For small $K$ values, the number of guard subcarriers is large, and thus there exist enough space in the frequency domain to avoid OOBE from neighboring sub-bands which is more advantageous to the SC-FDMA modulation. However, as K increases, where frequency spectrum utilization efficiency become highers, the number of guard band subcarriers becomes smaller, hence GFDM exhibits higher sum-rates.

## 4 Simulation with frequency selective channel.

There exist several differences on the simulation in this section compared to the the simulation with AWGN channel in the previous section.

1. The channel between the transmitter and receiver is frequency selective. The interfering channel from the unwanted user to the receiver is also frequency selective.

2. The spectral efficiency is calculated on a user $\hat{u}$ while the other users are all considered as the sources of interferences. In other words, for one trial of signal and interference generation, the spectral efficiency of one symbol block at the user $\hat{u}$ is calculated.

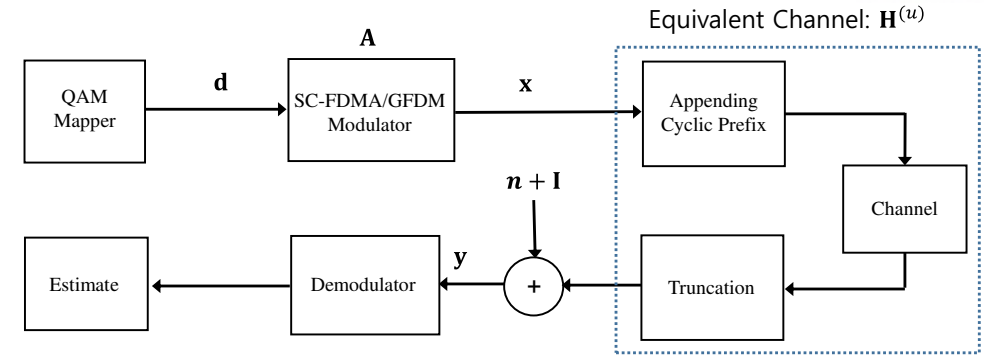


(a)

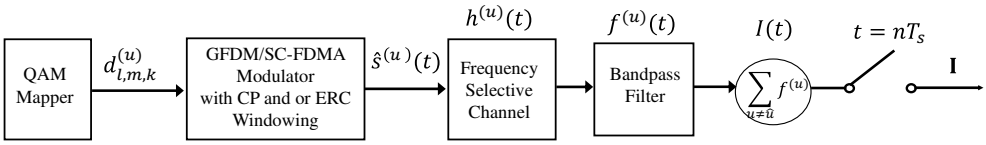


(b)

Figure 10: (a)The block diagram of transceiver in frequency selective channel. (b)The block diagram on inter-user interference generation.

3. Continuous signal of SC-FDMA and GFDM in (3), (7) are used to generate interference.

4. The discrete-time SC-FDMA and GFDM demodulator employs $K$ samples instead of $K_T$ samples to obtain estimate. For removing the aliasing among the bands, the ideal band pass filter is assumed with the relatively low $K$ samples.

5. The demodulation scheme of SC-FDMA signals is zero-forcing as the closed form of the correlation is not derived.

## 4.1 System Model

The transceiver design of GFDM or SC-FDMA in frequency selective channel is drawn in figure 10a. Note that the notation indicating user, $u$, disappeared as the spectral efficiency is calculated on a symbol block of a specific user, namely, user $\hat{u}$.

$$\mathbf{y} = \mathbf{H}\mathbf{x} + \mathbf{n} + \mathbf{I}, \tag{22}$$

where $\mathbf{H}$ is the $(KM \times KM)$-dimensional discrete-time circulant equivalent channel on the desired signal from user $\hat{u}$ to the reciever, and $\mathbf{I} \in \mathbb{C}^{KM \times 1}$ is the inter-user interference signal on decoding the signal from user $\hat{u}$ [28]. The variable $\mathbf{I}$ is formed by the signals from all users except $\hat{u}$ as described in figure 10b. In the figure 10b, each interfering signal $\hat{s}^{(u)}$ by user $u$ passes through

the interference channel, $h^{(u)}(t)$, and the bandpass filter for user $\hat{u}$, $f(t)$, as described in figure 10b [20, 22]. The sum of the continuous inter user interference after the channel and bandpass filter is denoted by $I(t)$, and is defined as

$$I(t) = \sum_{u \neq \hat{u}} \hat{s}^{(u)}(t) * h^{(u)}(t) * f(t). \tag{23}$$

The interfering signal, $\hat{s}^{(u)}$, is designed as the consecutive SC-FDMA or GFDM signals given in (3) and (7), i.e.,

$$\hat{s}^{(u)}(t) = \begin{cases} \sum_{l=-L}^{L} s_{l,GFDM}^{(u)}(t - lT_b) & \text{for GFDM signal} \\ \sum_{l=-L}^{L} s_{l,SC-FDMA}^{(u)}(t - lT_b) & \text{for SC-FDMA signal} \end{cases} \tag{24}$$

Here, instant signal at the time-point $t'$, $\hat{s}^{(u)}(t')$, can produce interference on the receiving window having duration $[t_1', t_2']$ even though $t' \notin [t_1', t_2']$ due to the time-domain spreading by convolution operation with the channel function and the bandpass filter. Therefore, the value of $L$ has to be set with consideration aforementioned. In the simulation, this value is set such that the value of the generation of the signal by convolution is less than $\frac{1}{80}$ of the signal near the receiving window.

The time-domain representation of ideal bandpass filter, $f(t)$, is designed to capture user $\hat{u}$'s frequency band only, and is given by

$$f(t) = \mathcal{F}^{-1}\left\{ \text{Rect}\left( \frac{f - \left(\frac{K-1}{2T_{fft}}\right)}{\left(\frac{K+1}{T_{fft}}\right)} \right) \right\}, \tag{25}$$

where the modulation matrix $\mathbf{A}$ for user $\hat{u}$ in figure (10b) is allocated with subcarrier sets $k \in \mathbb{K}^{(\hat{u})} = \{0, 1, \cdots, K-1\}$.

The continuous-time function of interference channel of $u$, $h^{(u)}(t)$, is assumed as frequency selective channel, i.e.,

$$h^{(u)}(t) = \sum_{i=1}^{N_h} a_i^{(u)} \delta\left(t - \tau_i^{(u)}\right). \tag{26}$$

where $\tau_i^{(u)}$ and $a_i^{(u)}$ are the time delay of the $i$-th tap of the channel and corresponding fading coefficient, respectively.

The vector $\mathbf{I}$, then, can be obtained by sampling the continuous-time interference signal with the sampling period of $T_s$ within the detecting window synchronized for $l = 0$ as $\Theta^{(\hat{u})} = 0$ at user $\hat{u}$;

$$\mathbf{I} = [\ I(0 \cdot T_s) \quad I(1 \cdot T_s) \quad \cdots \quad I((KM-1)T_s)\ ]^T. \tag{27}$$

### 4.2 Spectral efficiency calculation

The received signal $\mathbf{y}$ is demodulated by the zero-forcing (ZF) equalizer. Specifically, from (22), the equalized signal is given by

$$\hat{\mathbf{d}} = \mathbf{d} + (\mathbf{AH})^{-1}(\mathbf{I} + \mathbf{z}). \tag{28}$$

The spectral efficiency of GFDM in is, then, calculated as

$$C_G = \frac{(1-\nu)}{T_b K} \sum_{n=1}^{KM} \log \left( 1 + \frac{P_{tr}}{E \left| [(\mathbf{AH})^{-1}(\mathbf{I} + \mathbf{n})]_{n,1} \right|^2} \right), \tag{29}$$

where $\nu$ is the portion of guard subcarriers in the system which is defined as $\nu = K_G/(K + K_G)$.

On the other hand, the spectral efficiency of SC-FDMA modulation with ZF equalization is calculated as [26]

$$C_S = \frac{(1-\nu)}{T_b K} \sum_{n=1}^{K} \log \left( 1 + \frac{P_{tr}}{K \cdot E \left| [(\mathbf{H})^{-1}(\mathbf{I} + \mathbf{n})]_n \right|^2} \right) \Bigg|_{M=1}. \tag{30}$$

### 4.3 Simulation results

Numerical simulations were evaluated to investigate the spectral efficiency of GFDM modulation and SC-FDMA modulation in asynchronous multiple-access with respect to i) SNR and ii) $\nu$. The spectral efficiency is evaluated with multiple signal configurations: CP-window SC-FDMA(CP-SC-FDMA), CP-window GFDM with $M = 3$(CP-GFDM $M = 3$), CP-window GFDM with $M = 5$(CP-GFDM $M = 5$), ERC-window SC-FDMA(ERC-SC-FDMA), ERC-window GFDM with $M = 3$(ERC-GFDM $M = 3$) and ERC-window GFDM with $M = 5$(ERC-GFDM $M = 5$).

It is assumed that the users are allocated $K$ subcarriers, and that $K_G$ guard subcarriers exist between any neighboring two users' spectra to suppress the interference by OOBE. In the user $\hat{u}$'s point of view, the major sources of interference are user $\hat{u} - 1$ and $\hat{u} + 1$, hence only these two interfering users are taken into account to model the interference signal. The parameters used in the simulations are summarized in table 3.

All the asynchronous multiple-access schemes considered show increasing spectral efficiency for increasing SNR as shown in figures 11a and 11b, where the number of guard subcarriers is fixed as $K_G = 1$ and $K_G = 6$, respectively.

On the low SNR interval of SNR $<$ 4dB where $K_G = 1$ in figure 11a, SC-FDMA modulation performs the best, followed by GFDM modulation with $M = 3$ and GFDM modulation with $M = 5$. The GFDM ZF demodulator with a larger $M$ value particularly suffers from noise enhancement, and hence the spectral efficiency is relatively low in the noise-dominant low SNR regime.

As SNR increases, however, GFDM modulation with $M = 3$ outstrips SC-FDMA modulation roughly at SNR = 4dB, since the inter-user interference becomes dominating noise over AWGN. In

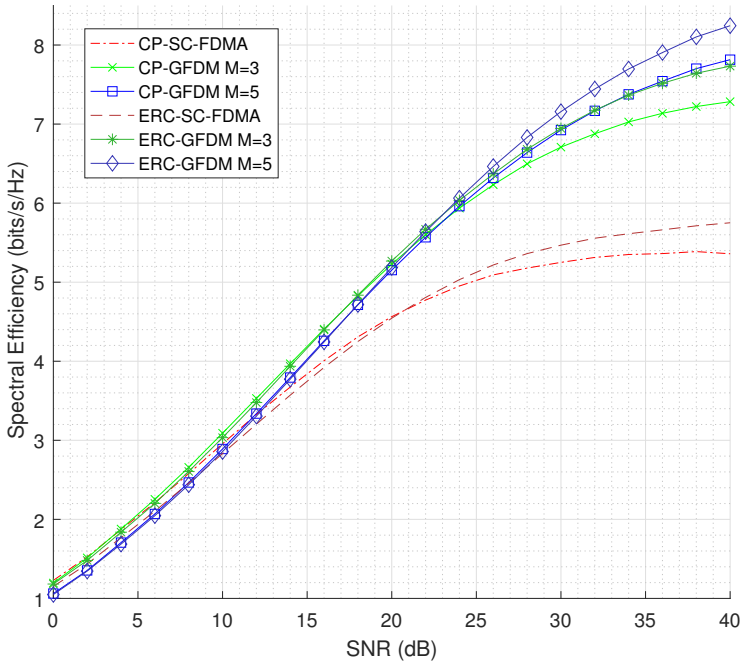


(a)

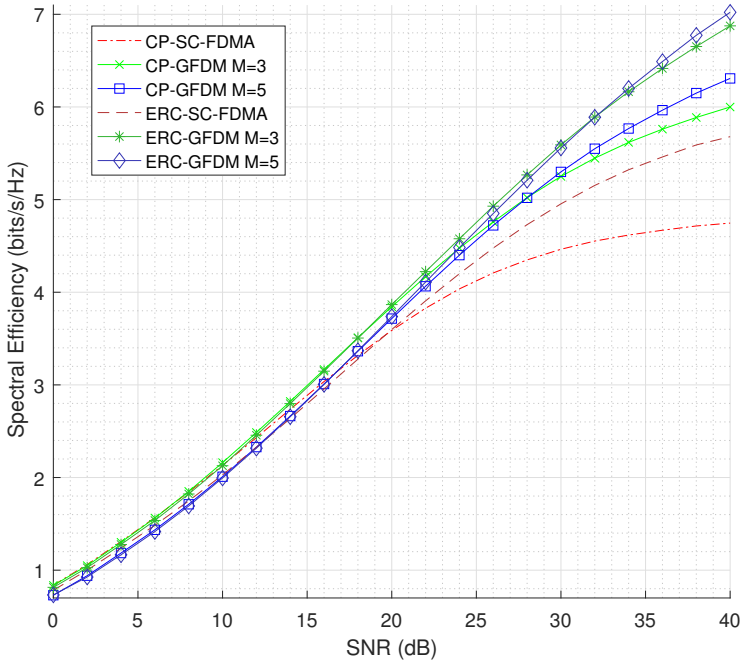


(b)

Figure 11: The spectral efficiency vs. signal-to-noise ratio(SNR) with (a) 1 guard subcarriers, and (b) 6 guard subcarriers.

Table 3: Parameters of simulation on frequency selective channel

| Parameters | Value |
|---|---|
| Number of Monte Carlo trials | 5000 |
| Time duration for a GFDM subsymbol ($T_{fft}$) | $66.7\mu s$ |
| Time duration for CP ($T_{CP}$) | $4.7\mu s$ |
| Time extension by windowing ($T_w$) | $4.7\mu s$ for windowed<br>$0s$ for non-windowed |
| Subcarrier spacing ($1/T_{fft}$) | $15kHz$ |
| Number of interfering users | 2 (nearest bands) |
| Number of subcarriers per user ($K$) | 10 |
| GFDM spectrum filter ($V_{filt}(f)$) | Raised cosine, $\alpha = 0.5$ |
| Windowing function ($w(t)$) | Expanded raised cosine |
| Time offset of the blocks of user $u$ ($\Theta^{(u)}$) | Uniform distribution $[0, T_b)$ |
| QAM modulation | BPSK |
| Number of paths of the frequency selective channel | 6 |
| Time delay of the $i$-th channel tab from user $u$ ($\tau_i^{(u)}$) | Uniform distribution$[0, 1.8\mu s)$ |
| Amplitude of the $i$-th channel tab corresponding to from user $u$ ($a_i^{(u)}$) | $R/\sqrt{6}$where $R$ is the unit Rayleigh random. |

the high SNR regime, interference dominates the where the GFDM modulation schemes significantly outperform the SC-FDMA modulation owing to lower OOBE, as seen from figure 4. In addition, for the same reason, the windowed schemes show higher performance than the non-windowed, and GFDM modulation with $M = 5$ outperforms GFDM modualtion with $M = 3$ in the high SNR regime.

In the case of $K_G = 6$, seen in figure 11b, the overall trends remain the same as in the $K_G = 1$ case. However, the spectral efficiency is decreased for all the schemes compared to figure 11a due to low usage of subcarriers, i.e., high $\nu$. In addition, reversal of superiority between GFDM and SC-FDMA modulations take place at higher SNR regime than in figure 11a as a result of reduced OOBE in SC-FDMA modulation.

With increasing $\nu$, inter-user interference become more mitigated. However, the frequency usage efficiency, $1 - \nu$, decreases. Hence, the overall frequency efficiency in (29), (30) cannot be expected to monotonically change with respect to $\nu$.

The spectral efficiency with respect to $\nu$ where SNR = 20dB is drawn in Fig 12. Spectral efficiency decreases as $\nu$ increases, except the increment from $\nu = 0\%$ to $\nu \approx 9.1\%$ in all schemes. The first increment is resulted from significant decrement of interference, while overall spectral efficiency diminishes owing to decreasing frequency usage, $1 - \nu$ in (29), (30).

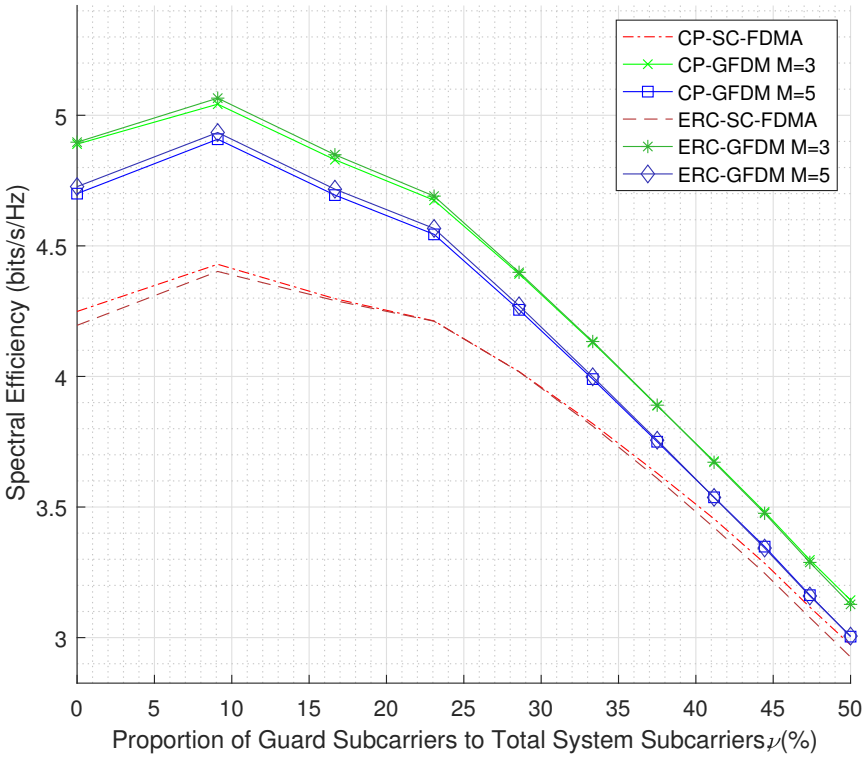


Figure 12: The spectral efficiency vs. proportion of guard subcarriers where signal to noise ratio is 20dB

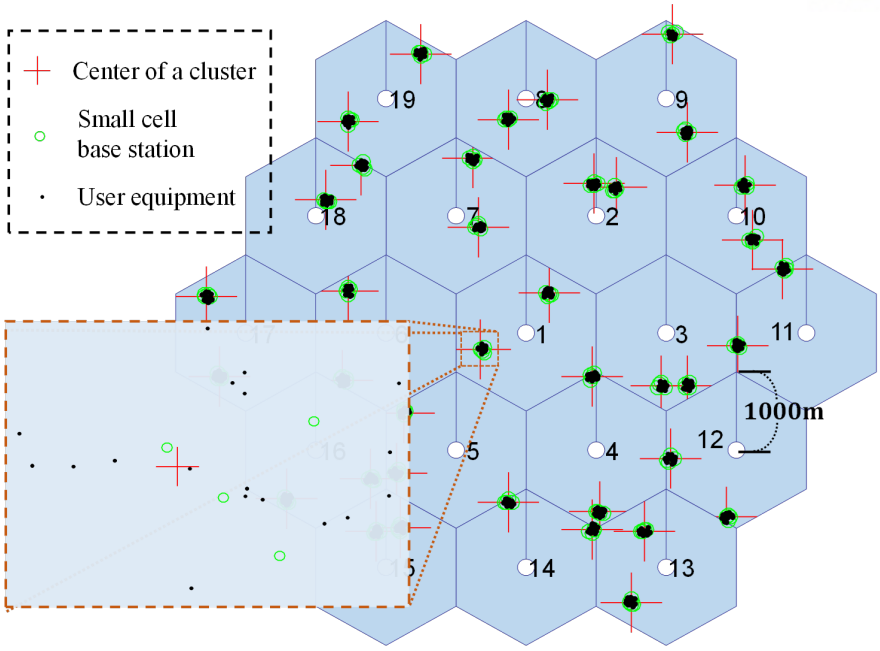


Figure 13: Macro cells and node dropping

# 5 System-Level Simulation

In this section, the spectral efficiency of the OFDM and GFDM modulation methods are compared by the numerical analysis in asynchronous uplink multiple-access by SLS. In particular, the small cell scenario in [3], which is one of the prominent technologies to enhance the throughput, is considered. SLS complies with 3GPP LTE standard Rel. 12 [4, 3, 5, 8] for the reference of small cell scenario, time parameters, and channel generation.

## 5.1 System model

### 5.1.1 BS & UE Dropping

Macro cell sectioning, small-cell base stations (BS) and randomly dropped users are illustrated in figure 13 following the parameters in table 4 [3]. Two tiers of macro interfering cells enclose macro cell 1, thus the uplink transmission to the BSs in the macro cell 1 are affected by the interference not only from users in the the macro cell 1, but also from the UEs in the other macro cells. On each macro cell, $N_{Cl}$ clusters are dropped. Each cluster contains $N_{SC}/N_{Cl}$ small-cell BSs and $N_U/N_{Cl}$ UEs where $N_{SC}$ and $N_U$ are multiples of $N_{Cl}$ and represent the number of small cell BSs per macro cell and the number of UEs per macro respectively.

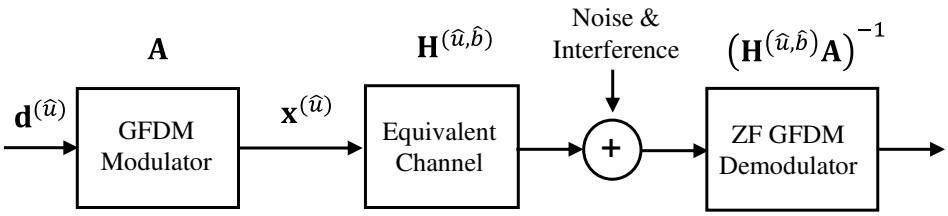


Figure 14: Block diagram of GFDM tranceiver for system-level simulation.

### 5.1.2 Transceiver Structure & Channel Generation

The GFDM and OFDM modulation matrix $\tilde{\mathbf{A}} \in \mathbb{C}^{K_T M \times K_T M}$ is defined in the Section 3.1. In addition, the OFDM modulator can be represented by $\mathbf{D}_{K_T}$ with $M = 1$. In the transceiver structure drawn in figure 14, the source of the desired signal to BS $\hat{b}$ is represented by UE $\hat{u}$. Thus, the signals from the UE $u$, $\neq \hat{u}$, transmitted to the BE $\hat{b}$ is affected as interference in the time synchronization condition is bad as explained in the Section 5.3.

The circulant equivalent channel from a source UE $u$,$\in \mathbb{U}=\{1, 2, \cdots, N_U\}$, to destination BS $b$,$\in \mathbb{B} = \{1, 2, \cdots, N_{SC}\}$, in figure 14 is defined as $\mathbf{H}^{(u,b)}$. The continuous-time small fading channel with six clusters of beam is designed following [4], and the path-loss and shadowing is designed in accordance with [3]. The continuous-time channel is, then, converted to the discrete channel to form $\mathbf{H}^{(u,b)}$.

Frequency representation of $\mathbf{H}^{(u,b)}$ provides us channel gain per subcarrier. Dividing total subcarriers into $N_{RB}$ resource blocks each of which is composed with neighboring subcarriers, channel gain at the resource block(RB) $r$ ($\in \mathbb{R} = \{1, 2, \cdots, N_{RB}\}$) of the channel from UE $u$ to BS $b$ is defined as $C_r^{(u,b)}$.

## 5.2 Uplink Resource Allocation

Depending on resource allocation scheme, distribution of signal to interference plus noise ratio (SINR) among allocated channels significantly varies. In this simulation, two resource allocation schemes, *Max SNR per small cell* and *Max updating SINR*, are compared.

Each BS contains $N_{RB}$ slots of RB, and each RB slot in a BS is able to accommodate one channel. Hence, once an RB slot in a BS is allocated to a UE, the RB cannot be allocated to another UE. Let's call this rule *single reception* in the sequel. On the other hand, UE can link with only one BS, and this constraint is called *single association*.

### 5.2.1 Max SNR per small cell

In this user resource allocation scheme, association of UE to BS and assignment of RB within a BS are operated in separated stages. First, each UE associates to a small cell BS $b$ which promises for the UE to have maximum throughput throughout all RBs in the BS $b$, calculated directly from $C_r^{(u,b)}$. Note this nominal throughput is different from the actual throughput in that it does not

**Algorithm 1** Max updating SINR

**Require:** $\delta$: minimum value of allocatable SINR, $\mathbb{U}$, $\mathbb{B}$, and $\mathbb{R}$: The sets of indices of UE, BS, and RB.

($Init$) $L \leftarrow \emptyset$: Set of allocated channel

$SI_r^{(u,b)} \leftarrow S_r^{(u,b)} \forall u \in \mathbb{U}, b \in \mathbb{B}, r \in \mathbb{R}$

**while** not all $SI_r^{(u,b)}$ is zero **do**

$(\bar{u}, \bar{b}, \bar{r}) \leftarrow \arg\max_{(u,b,r)} SI_r^{(u,b)}$

$SI_{\bar{r}}^{(u,b)} \leftarrow SI_{\bar{r}}^{(u,b)} \left( \frac{S_{\bar{r}}^{(u,b)}}{S_{\bar{r}}^{(u,b)} + SI_{\bar{r}}^{(u,b)} \cdot S_{\bar{r}}^{(\bar{u},\bar{b})}} \right) \forall u \in U,\ b \in B$

$SI_r^{(u,\bar{b})} \leftarrow 0 \forall r \in R, u \in U \backslash \{\bar{u}\}$ *single association rule*

$SI_r^{(\bar{u},b)} \leftarrow 0 \forall r \in R, b \in B \backslash \{\bar{b}\}$ *single reception rule*

$SI_{\bar{r}}^{(\bar{u},\bar{b})} \leftarrow 0$ *excluding not to be selected again*

**for** $u \in U$, $b \in B$ $r \in R$

**if** $SI_r^{(u,b)} < \delta$ **then**

$SI_r^{(u,b)} \leftarrow 0$

**end if**

**end for**

$L \leftarrow L \cup \{(\bar{u}, \bar{b}, \bar{r})\}$

**end while**

**Return** $L$

consider interference. RBs at the BS $b$ are allocated to the UEs associated with the BS $b$ by round robin scheduling. If there does not exist UE associated with a BS, the RBs in the BS are allocated to nowhere, that is, the BS becomes inactive.

### 5.2.2 Max updating SINR

Exploiting SINR information for all resource allocation cases, we can achieve optimal spectral efficiency. However this method is impossible in practical due to complexity. Hence we suggest a practical algorithm having complexity while it still is able to exploit SINR information.

The max updating SINR algorithm is described in Algorithm 1. In this algorithm, one RB of all BSs is assigned to a UE at one round, and the operation is conducted repeatedly while SINR is updated for each round until there exist allocable RBs. Let $S_r^{(u,b)}$ be the SNR value for possible link from UE $u$ to BS $b$ via RB $r$. Similarly, $SI_r^{(u,b)}$, which represents SINR value for possible link from UE $u$ to BS $b$ via RB $r$, is derived by SNR considering noise term as the sum of AWGN and all interference generated from sources that have been already allocated. The set of allocated channels, $L$, is composed with triples $(u, b, r)$ and is given by Algorithm 1.

## 5.3 Interference Modeling

Throughout the resource allocation, UEs' uplink channels are determined as $L$. Let the indices $\hat{u}(\in \mathbb{U})$ and $u(\in \mathbb{U} \backslash \{\hat{u}\})$ indicate, hereafter, a UE for throughput calculation and its interferer

respectively. The signal-to-interference-plus-noise ratio(SINR) of the desired signal comes from UE $\hat{u}$ considering UE $u$'s signal as a source of interference.

Matrix $\hat{\mathbf{A}}^{(u)} \in \mathbb{C}^{N_T \times KM}$ denotes CP-attached resource-block-selective GFDM modulation matrix for UE $u$, where $N_T$ represents the number of discrete-time domain samples in a symbol block including CP. The matrix $\hat{\mathbf{A}}^{(u)}$ is constructed by attaching CP in front of the first row of $\tilde{\mathbf{A}}$, then embedding zero elements in the columns which correspond to symbols unoccupied by UE $u$. This zero-padding method is difference to the zero-padding in the 3.1 in that the zeros are inserted to the columns of non-used symbols, not to the symbols them selves.

Two consecutive CP-attached interfering discrete-time transmit signals from UE $u$ are denoted by a $(2N_T \times 1)$-dimensional vector

$$\mathbf{x}'^{(u)} = \mathbf{A}'^{(u)}\mathbf{d}'^{(u)} = \begin{bmatrix} \hat{\mathbf{A}}^{(u)} & \mathbf{0} \\ \mathbf{0} & \hat{\mathbf{A}}^{(u)} \end{bmatrix} \begin{bmatrix} \mathbf{d}_0^{(u)} \\ \mathbf{d}_1^{(u)} \end{bmatrix}, \tag{31}$$

where $\mathbf{A}'^{(u)} = \mathbf{J}_2 \otimes \hat{\mathbf{A}}^{(u)}$ and $\mathbf{d}'^{(u)} = [\mathbf{d}_0^{(u)\mathrm{T}}\, \mathbf{d}_1^{(u)\mathrm{T}}]^{\mathrm{T}}$. Here, $\mathbf{J}_a$ represents $a$ by $a$ identity matrix, $\otimes$ represents Kronecker product, and $\mathbf{X}^{\mathrm{H}}$ represents and Hermitian matrix of $\mathbf{X}$. An important observation in (31) is that the asynchronously transmitted interfering signal is represented by the signal which is generated by modulation of a vector of QAM symbol vector, $\mathbf{d}'^{(u)}$. Since the QAM symbols are assumed to be i.i.d., the closed form of the expected power of any linear transform of the signals is able to be calculated as follows.

The interference signal generated by UE $u$ to BS $\hat{b}$ is transmitted via interference channel from $u$ to $\hat{b}$, $\mathbf{H}^{(u,\hat{b})}$. In asynchronous multiple-access, detection of signal from different UEs requires different synchronization of detection windows. Let $\Theta_{\hat{u}}^{(u)}$ $(\in [1, N_T])$ denote the starting position of detection window for UE $\hat{u}$ within discrete-time sample points of the received interference signal, $\mathbf{H}^{(u,\hat{b})}\tilde{\mathbf{x}}^{(u)}$. The received interference from UE $u$ truncated by detection window for UE $\hat{u}$ is defined as;

$$\mathbf{i}_{\hat{u}}^{(u,\hat{b})} = \mathbf{T}_{\hat{u}}^{(u)}\mathbf{H}^{(u,\hat{b})}\mathbf{A}'^{(u)}\mathbf{d}'^{(u)}, \tag{32}$$

where $\mathbf{T}_{\hat{u}}^{(u)}$ represents truncation matrix defined as $\mathbf{T}_{\hat{u}}^{(u)} = [\,\mathbf{0}_{N,\Theta_{\hat{u}}^{(u)}}\, \mathbf{J}_N\ \mathbf{0}_{N,N\Theta_{\hat{u}}^{(u)}}\,]^{\mathrm{T}}$. Here, $\mathbf{0}_{a,b}$ represents $a$ by $b$ matrix in which elements are all zeros. Note that $\mathbf{i}_{\hat{u}}^{(u,\hat{b})}$ includes cases whether BS $\hat{b}$ is the destination of UE $u$ or not. In other words, inter-carrier interference and inter-small-cell interference are both represented by $\mathbf{i}_{\hat{u}}^{(u,\hat{b})}$, hence let's call it inner-macro cell interference.

Let $\mathbf{z}_{\hat{u}}^{(u,\hat{b})}$ represent interference from UE $u$ after zero-forcing demodulation for UE $\hat{u}$ at BS $\hat{b}$ in figure (14).

$$\mathbf{z}_{\hat{u}}^{(u,\hat{b})} = (\mathbf{H}^{(\hat{u},\hat{b})}\mathbf{A})^{-1}\mathbf{i}_{\hat{u}}^{(u,\hat{b})} = \mathbf{Q}_{\hat{u}}^{(u,\hat{b})}\tilde{\mathbf{d}}^{(u)} \tag{33}$$

where $\mathbf{Q}_{\hat{u}}^{(u,\hat{b})} = (\mathbf{H}^{(\hat{u},\hat{b})}\mathbf{A})^{-1}\mathbf{T}_{\hat{u}}^{(u)}\mathbf{H}^{(u,\hat{b})}\mathbf{A}'^{(u)}$. Power of total inner-macro-cell interference at each symbol detection (i.e, at specific subcarrier and subsymbol) after zero-forcing for UE $\hat{u}$ is derived

as each element of the vector $\mathbf{P}_{inner}^{(\hat{u})}$.

$$\begin{aligned}\left[\mathbf{P}_{inner}^{(\hat{u})}\right]_{i,1} &= \left[\mathrm{E}\left[\sum_{u\in U\setminus\{\hat{u}\}} \mathbf{z}_{\hat{u}}^{(u,\hat{b})}(\mathbf{z}_{\hat{u}}^{(u,\hat{b})})^{\mathrm{H}}\right]\right]_{i,i} \\ &= \left[\sum_{u\in U\setminus\{\hat{u}\}} P_t\mathbf{Q}_{\hat{u}}^{(u,\hat{b})}(\mathbf{Q}_{\hat{u}}^{(u,\hat{b})})^{\mathrm{H}}\right]_{i,i} \end{aligned} \tag{34}$$

Another interference injected to a receiver is inter-macro-cell interference, coming from other cells' uplink transmission as seen in Fig. 13. As there exist a large number of interfering signals coming from outside of the macro cell, and they have small power, let they be designed by Gaussian random variable multiplied by pathloss of the channel assuming ergodicity. The vector of total interference power on detection of signals $\hat{u}$ combining powers of inter-macro-cell and inner-macro-cell interference is denoted by $\mathbf{P}_{sum}^{(\hat{u})}$.

### 5.4 Spectral Efficiency Calculation

Spectral efficiency per small cell, $SE$, is calculated as [1]

$$SE = \frac{1}{BN_{SC}} \sum_{\hat{u}\in U} \sum_{j\in J^{(\hat{u})}} \frac{1}{T_s} \log\left(1 + \frac{P_t}{N_o + \left[\mathbf{P}_{sum}^{(\hat{u})}\right]_{j,1}}\right), \tag{35}$$

where $T_s$ is total time duration of a symbol, $B$ is bandwidth of the multiple-access system, $J^{(\hat{u})}(\subset \{1, 2, \cdots, N\})$ is set of indices for symbols allocated to UE $\hat{u}$, and $N_0$ represents variance of AWGN. In GFDM case, $J^{(\hat{u})}$ is a set of all function values corresponding to couple ($m$,$k$) which conveys symbols of UE $\hat{u}$. Note that domain of $k$ is determined by resource allocation.

### 5.5 Simulation Results

The simulation evaluated spectral efficiency of GFDM and OFDM using two resource allocation algorithms varying $N_{UE}$ from 20 to 80 with increment 10. Simulation arameters are listed in Table 4.

The result in Fig. 15 shows GFDM outperforms OFDM throughout all user density on both resource allocation schemes. We infer lower OOBE of GFDM than that of OFDM reduces ICI, which enhances the spectral efficiency.

Comparing two resource allocation schemes, max SNR per small cell shows better performance on low user density regime where number of UE is less than 40, whereas max updating SINR shows higher performance with a large number of UEs more than 50. In max SNR per small cell scheme, as more packed interfering UE by increasing $N_U$, ignorance of interference impacts marginal declination of the spectral efficiency. On the other hand, max updating SINR has advantage as $N_U$ increases

Table 4: Parameters of system-level simulation

| **Parameter** | **Value** |
|---|---|
| # (the number of) trials | 100 |
| Spatial channel | SISO |
| *Parameters on node dropping [3]* | |
| # clusters, $N_{Cl}$ | 2 |
| # small cell BS per cluster, $N_{SC}$ | 4 |
| Rough # UE, $N_{UE}$ | *Variable*: 20~80 (increment by 10) |
| Activation of macrocell BS | No |
| *Parameters on GFDM modulation* [2, 8, 28, 25] | |
| Bandwidth | 2.5 MHz |
| Sampling frequency | 3.84 MHz |
| # occupied subcarriers | 144 |
| # resource blocks (RB) | 12 |
| # subcarriers per RB | 12 |
| # guard subcarrier per RB | 1 |
| # sampling points per GFDM subsymbol $K$ | 256 |
| # GFDM subsymbols, $M$ | 3 |
| Time duration CP Length | $4.7\mu s$ (short CP) |
| Time duration for a GFDM subsymbol | $66.7\mu s$ |
| Total time duration for a GFDM symbol, $T_s$ | 204.8 $\mu s$ |
| Samples of a GFDM symbol including CP, $N_T$ | 780 |
| Transmit power of UE, $P_t$ | 23 dBm |
| Noise variance, $N_0$ | -109 dBm |

Table 5: Gain of GFDM depending on resource allocation schemes.

| Number of UEs | 20 | 30 | 40 | 50 | 60 | 70 | 80 |
|---|---|---|---|---|---|---|---|
| max SNR | 4.7 | 4.1 | 4.2 | 4.9 | 4.4 | 4.0 | 4.2 |
| max updating SINR | 8.4 | 8.7 | 9.5 | 9.9 | 10.0 | 10.3 | 10.8 |

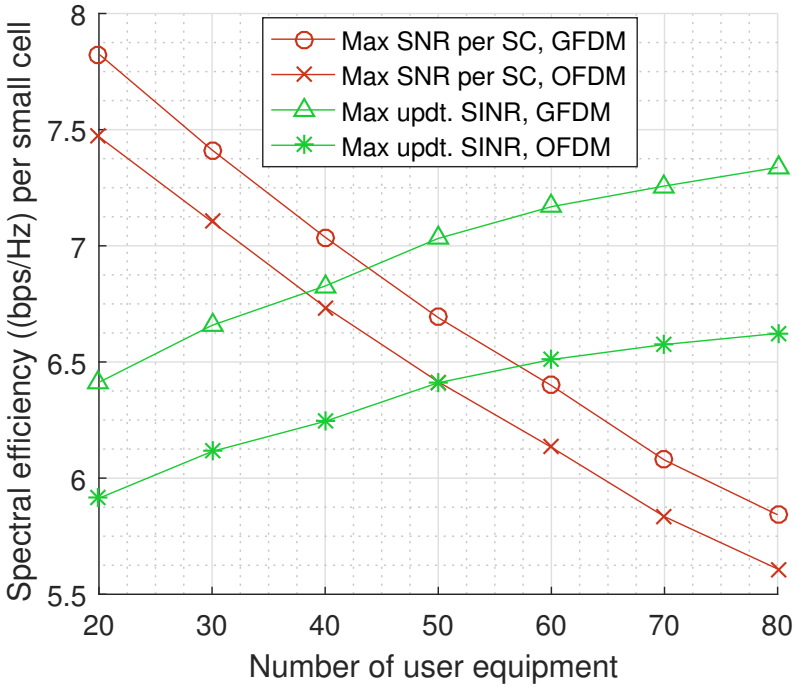


Figure 15: Spectral efficiency of GFDM and OFDM using two resource allocation scheme.

since the number of inactive RBs, which is rejected to be linked by lower SINR than threshold $\delta$, decreases due to good channel conditions.

Table. 5 shows percent gain of spectral efficiency using GFDM than using OFDM as $N_U$ increases. GFDM has small OOBE, which means small ICI, hence have advantageous where influence of interference is significant i.e., where $N_U$ is large.

# 6 Conclusion

In this thesis, the throughput performance of the GFDM and conventional modulation methods, such as SC-FDMA and OFDM, are compared in the asynchronous uplink multiple-access environment. The results of LLS conducted with AWGN and frequency selective channel show that GFDM outperforms SC-FDMA modulation in the high-SNR regime as GFDM has lower OOBE than SC-FDMA. On the other hand, it is observe that GFDM has lower throughput in the the low-SNR regime due to the noise enhancement using zero-forcing demodulation. In addition, the plot of throughput versus the number of guard subcarriers is non-monotonic as the increment of guard subcarrier has both effects: lowering inter-user interference, and lowering spectrum usage rate.

The SLS on asynchronous uplink multiple-access in small cell scenario shows 4% to 10% gain of GFDM compared to OFDM depending on the uplink resource allocation scheme. This result corresponds to the observations of the LLS; GFDM shows better performance due to the high SNR

guaranteed by small cell.

# References


[1] Requirements related to technical performance for IMT-Advanced radio interface(s). Technical report, ITU-R, ITU-R, Geneva, Switzerland, Tech. Rep. M.2134, 2008.

[2] Guidelines for evaluation of radio interface technologies for IMT-Advanced. Technical report, ITU-R, Geneva, Switzerland, Tech. Rep. M.2135-1, 2009.

[3] Small cell enhancements for E-UTRA and E-UTRAN - physical layer aspects. Reprot TR 36.872 v12.1.0, 3GPP, 2013.

[4] Spatial channel model for multiple Input multiple output (MIMO) simulations. Technical report, 3GPP, Valbonne, France, Tech. Rep. TR 25.996 v12.0.0, Sept. 2014.

[5] Evolved universal terrestrial radio access (E-UTRA); physical channels and modulation (Release 12). Standard TS 36.211 V12.8.0, 3GPP, 2015.

[6] IMT Vision - Framework and overall objectives of the future development of IMT for 2020 and beyond. Report Rec. ITU-R M.2083-0, ITU - R, 2015.

[7] Evolved universal terrestrial radio access (E-UTRA); multiplexing and channel coding (Release 12). Standard TS 36.213 V12.10.0, 3GPP, 2016.

[8] Evolved universal terrestrial radio access (E-UTRA); physical layer procedures (Release 12). Standard TS 36.213 V12.10.0, 3GPP, 2016.

[9] S. Ahmadi. *LTE-Advanced: A Practical Systems Approach to Understanding 3GPP LTE Releases 10 and 11 Radio Access Technologies.* Academic Press. Elsevier Science & Technology Books, 2013.

[10] Jeffrey G. Andrews, Stefano Buzzi, Wan Choi, Stephen V. Hanly, Angel Lozano, Anthony C. K. Soong, and Jianzhong Charlie Zhang. What will 5G be? *IEEE J. Sel. Areas Commun.*, 32(6):1065–1082, June. 2014.

[11] M. Debbah. Short introduction to OFDM. Report, Alcatel-Lucent.

[12] Gerhard Fettweis. GFDM - generalized frequency division multiplexing. In *Proc. IEEE Veh. Technol. Conf.*, Barcelona, Spain, Apr. 2009.

[13] Gerhard P. Fettweis. The tactile Internet: applications and challenges. *IEEE Veh. Technol. Mag.*, 9(1):64–70, Mar. 2014.

[14] G. Wunder *et al.* 5GNOW: non-orthogonal asynchronous waveforms for future mobile applications. *IEEE Commun. Mag.*, 52(2):97 – 105, Feb. 2014.

[15] Ivan Gaspar, Nicola Michailow, Ainoa Navarro, Eckhard Ohlmer, Stefan Krone, and Gerhard Fettweis. Low complexity GFDM receiver based on sparse frequency domain processing. In *Proc. IEEE Veh. Technol. Conf.*, Dresden, Germany, June 2013.

[16] John A. Gubner. *Probability and random processes for electrical and computer engineers*. Cambridghe Univ. press, 2006.

[17] P. H. Lehne and F. Bohagen. OFDM(A) for wireless communication. Report, Telenor R&I, 2008.

[18] M. MatthÃ©, L. L. Mendes, and G. Fettweis. Asynchronous multi-user uplink transmission with generalized frequency division multiplexing. In *2015 IEEE International Conference on Communication Workshop (ICCW)*, pages 2269–2275, June 2015.

[19] Maximilian Matthe, Nicola Michailow, Ivan Gaspar, and Gerhard Fettweis. Influence of pulse shaping on bit error rate performance and out of band radiation of generalized frequency division multiplexing. In *IEEE Int. Conf. Commun. Workshops*, Sydney, Australia, June 2014.

[20] Y. Medjahdi, M. Terre, D. Le Ruyet, D. Roviras, and A. Dziri. The impact of timing synchronization errors on the performance of OFDM/FBMC systems. In *2011 IEEE International Conference on Communications (ICC)*, pages 1–5, June 2011.

[21] Yahia Medjahdi, Michel Terre, Didier Le Ruyet, and Daniel Roviras. Asynchronous OFDM/FBMC interference analysis in selective channels. In *Proc. IEEE 21st Int. Symp. on personal indoor and mobile radio commun.*, pages 538 – 542, Istanbul, Turkey, Sept. 2010.

[22] Yahia Medjahdi, Michel Terre, Didier Le Ruyet, Daniel Roviras, and Ali Dziri. Performance Analysis in the Downlink of Asynchronous OFDM/FBMC Based Multi-Cellular Networks. *IEEE Trans. on Wireless Commun.*, 10(8):2630–2639, Aug. 2011.

[23] Yahia Medjahdi, Michel Terre, Didier Le Ruyet, Daniel Roviras, Josef Nossek, and Leonardo Gomes Baltar. Inter-cell interference analysis for OFDM/FBMC systems. In *Proc. IEEE 10th Workshop on Signal Process. Advances in Wireless Commun.*, pages 598–602, Jun. 2009.

[24] N. Michailow, S. Krone, M. Lentmaier, and G. Fettweis. Bit error rate performance of generalized frequency division multiplexing. In *2012 IEEE Vehicular Technology Conference (VTC Fall)*, pages 1–5, Sept 2012.

[25] Nicola Michailow, Maximilian Matthe, Ivan Simoes Gaspar, Ainoa Navarro Caldevilla, Luciano Leonel Mendes, Andreas Festag, and Gerhard Fettweis. Generalized frequency division multiplexing for 5th generation cellular networks. *IEEE Tran. Commun.*, 62:3045 – 3061, Sept. 2014.

[26] H. G. Myung, J. Lim, and D. J. Goodman. Single carrier FDMA for uplink wireless transmission. *IEEE Vehicular Technology Magazine*, 1(3):30–38, Sept 2006.

[27] H.G. Myung and D.J. Goodman. *Single-carrier FDMA: a new air interface for Long Term Evolution*. Wireless Communications and Mobile Computing. Wiley, 2008.

[28] Woojin Park and Hyun Jong Yang. On spectral efficiency of asynchronous GFDMA and SC-FDMA in frequency selective channels. In *Proc. IEEE Veh. Technol. Conf. Spring*, Nanjing, China, May 2016.

[29] Woojin Park, Hyun Jong Yang, and Hyunmyung Oh. Sum-rates of asynchronous GFDMA and SC-FDMA for 5G uplink. *ICT Express*, 1(3):127 – 131, Dec. 2015.

[30] R. Prasad. *OFDM for Wireless Communications Systems*. Artech House universal personal communications series. Artech House, 2004.

[31] Xiang Gen Xia. A family of pulse-shaping filters with ISI-free matched and unmatched filter froperties. *IEEE Trans. on Commun.*, 45:1157–1158, Oct. 1997.

## Acknowledgment

For two years of my master pursuit and a year of my undergraduate research, I have been taught by professor Hyun Jong Yang with his invaluable advice. I could learn communication systems in depth and professionalism seeing his endless passion on the communication system field. Now, I can recognize the advice has made me improve myself to become more valuable person. Let me convey immeasurable gratitude to my adviser taking a space in this paper. In addition, I want to deliver thanks to professor Hyoil Kim and Jin-Ho Chung for the advisement on writing this paper and the evaluation of my presentation.

To my excellent colleagues in the laboratory. Hyun Myung, thank you for sharing the knowledge about the project you had been doing. You have great passion on the field, and I hope you achieve what you want to achieve. Myeung Un, thank you for making the lab more harmonized. You have remarkable endurance to pursuit something, so I expect you do well in the remaining period of your Ph.D pursuit. Yeungjun, your passion and creativity on work made me stimulated to perform more. You can take advantage of these strong points on research. Youjin, it was very helpful for me that you gave me advice based on your keen observations. You are smart and reasonable, so you can be successful on whatever you will do. Jong Gyu, thank you for helping me to solve challenging mathematical problems based on your excellent math skills. Kiyoon, you were so patient when you were teaching me on Linux system although it may be annoying to you. I could get many knowledge about computer programming. I hope you, Jong Gyu and Kiyoon, can use your expertise to the communication system field. Under the dedicated professor, you all can learn and master what you are, and will be researching. I hope we see at the top.

Thanks to all my friends. Sometimes you helped me what I could not do alone, sometimes you shared your experiences that I had not had, and sometimes you made me feel easy giving me nothing but casual words. I'm sorry about that I am a kind of man who does not call you before you call me.

To my family. Your supports originated from the love are always more than what others could give. Lets keep our health.